Check for updates

Continuous biphasic chemical processes in a four-phase segmented flow reactor†

Amanda A. Volk, [iD] [a] Robert W. Epps, [iD] [a] Daniel Yonemoto, [b] Felix N. Castellano [iD] [b] and Milad Abolhasani [iD] *[a]

A quaternary segmented flow regime for robust and flexible continuous biphasic chemical processes is introduced and characterized for stability and dynamic properties through over 1500 automatically conducted experiments. The flow format is then used for the continuous flow ligand exchange of cadmium selenide quantum dots under high intensity ultraviolet illumination for improved photoluminescence quantum yield.

Microfluidic chemical synthesis, which has emerged as a material- and time-efficient alternative to conventional flask-based syntheses, is finding roles in an increasing number of reactive systems, spanning pharmaceutical research,[1] catalysis,[2,3] and organic/inorganic materials syntheses[4-10] due to the propensity for automation, low reagent consumption, and precise heat/mass transfer properties. In these studies, efforts have transitioned from single-phase flow systems into more complex multi-phase flow (MF) formats. Although single-phase flow formats are simpler to implement, they suffer from poor reagent mixing due to axial dispersion and diffusion limited mass transfer. In addition, single phase systems are prone to fouling of microreactor channels, thereby limiting microreactor lifetime. Compared to single-phase systems, MF formats have enhanced mass transfer rates due to internal recirculation within reactant droplets,[11,12] leading to uniform and controlled reaction environments and accelerated kinetics (i.e., decreased synthesis times).[13,14] Precise tuning of mass transfer dynamics within reactive MF systems has led to accurate fundamental and kinetic studies of reactions with fast kinetics[15] and the formation of materials that would otherwise be unachievable in equivalent flask reactors. In

addition, some MF formats are amenable to sequential injection of reactant phases, enabling multi-stage reactions to be performed continuously in flow.[16]

Despite the advantages of MF flow reactors, currently, MF formats without fouling – an important requirement for reliable and continuous automated/autonomous experimentation in the rapidly emerging field of digitalization of reaction engineering[5,8,17-22] – are limited to single reactive phase systems. This limitation has prevented the development of robust liquid–liquid biphasic reaction systems in continuous flow reactors and their further adoption by autonomous experimentation strategies.

Among interfacial biphasic reactions, ligand exchange reactions have been used to functionalize and improve the performance of colloidal nanocrystals, including cadmium selenide (CdSe) quantum dots (QDs).[23,24] Although there are some concerns about the toxicity of cadmium-based devices, currently, CdSe QDs remain of significant interest because of their desirable optical and optoelectronic properties. The biphasic ligand exchange of bulky organic capping ligands with short ionic ligands, such as S^{2-}, can further expand the application and performance of CdSe QD-based devices by improving interparticle coupling and solution processability.[24,25] However, S^{2-}-capped CdSe QDs after the biphasic ligand exchange typically exhibit significantly lower PL intensity, likely due to the introduction of surface defects.[26] A robust experimental strategy which can not only be used for the continuous flow biphasic ligand exchange of CdSe QDs, but enhance QD performance post-ligand exchange, is necessary to optimize the performance of ligand exchanged colloidal nanocrystals through automated high-throughput experimentation integrated with a multimodal in situ nanocrystal characterization probe.

To date, segmented MF can be categorized into two- and three-phase formats.[8,10,27-29] Two-phase systems include immiscible liquid–liquid (L_2) and liquid–gas (LG) flow, and three-phase systems include immiscible liquid–liquid–liquid (L_3) and liquid–liquid–gas (L_2G) flow. In many chemical

[a] Department of Chemical and Biomolecular Engineering, North Carolina State University, 911 Partners Way, Raleigh, NC 27695-7905, USA.
E-mail: abolhasani@ncsu.edu; Web: www.abolhasanilab.com
[b] Department of Chemistry, North Carolina State University, 911 Partners Way, Raleigh, NC 27695-7905, USA
† Electronic supplementary information (ESI) available. See DOI: 10.1039/d1re00247c

processes, it is necessary to separate the reactive solutions from the microchannel wall to avoid fouling and eventually clogging of the microreactor.[14,30,31] The gradual material build-up in the microchannel may be eliminated through the inclusion of immiscible inert liquids – referred to as inert carrier phases – which preferentially wet microreactor surfaces. Consequently, single phase reactive systems may be explored through L_2, L_3, and L_2G flow formats without concerns over channel fouling. Similarly, reactive biphasic systems may be explored through L_3 formats which can have two reactant phases and one inert carrier phase. However, the L_3 format, compared to L_2 and L_2G systems, has limited operational windows (reactive phase ratios, droplet velocities, and reactor dimensions) due to droplet coalescence and uncontrollable phase combination. A flow configuration which combines the robust operational window of gas–liquid MFs and the operational longevity of L_2-carrier phase formats is therefore needed to realize the application of continuous microfluidic reactors to biphasic processes.

Recently, the commercial availability of microscale fluoropolymer tubing, as well as various cross junctions and fittings, have made construction of modular flow chemistry platforms using MF formats readily accessible to a wide range of research labs. The modularity of tube-based microreactors, in contrast to microfabricated reactors, enables rapid system reconfiguration to efficiently test various flow configurations and formats in a matter of seconds. Implementation of these tube-based microreactors has unlocked greater control and flexibility in the study and development of reactive processes in flow, while reducing the time and cost required to build and redesign flow chemistry platforms for fundamental and applied studies of multi-phase chemical processes. In this work, we introduce a quaternary segmented flow (QSF) format, using commercially available junctions and tubing, for continuous flow biphasic reactions. We extensively characterize the operational conditions necessary to attain stable QSF through 810 automated experiments with inline spectral monitoring and compare these conditions to three different flow formats through 765 additional experiments. Compared to existing MF formats, this 4-phase MF can match the operational envelope of L_2G three-phase flow, while eliminating microreactor fouling. We then demonstrate the continuous flow biphasic ligand exchange of CdSe QDs through this robust QSF format using the same experimental sampling system and automated reference collection to account for the continuously changing carrier solution absorption. In addition to introducing QSF and continuous-flow biphasic ligand exchange for the first time, we also demonstrate the capability of continuous flow photo-enhanced ligand exchange, which produces S^{2-}-capped CdSe QDs with improved PL intensities.

In the first set of experiments, we evaluated the accessible operational envelopes of each of the four flow regimes available for biphasic reaction studies (i.e., L_2, L_3, L_2G, and QSF) using a polar protic solvent (formamide), a nonpolar
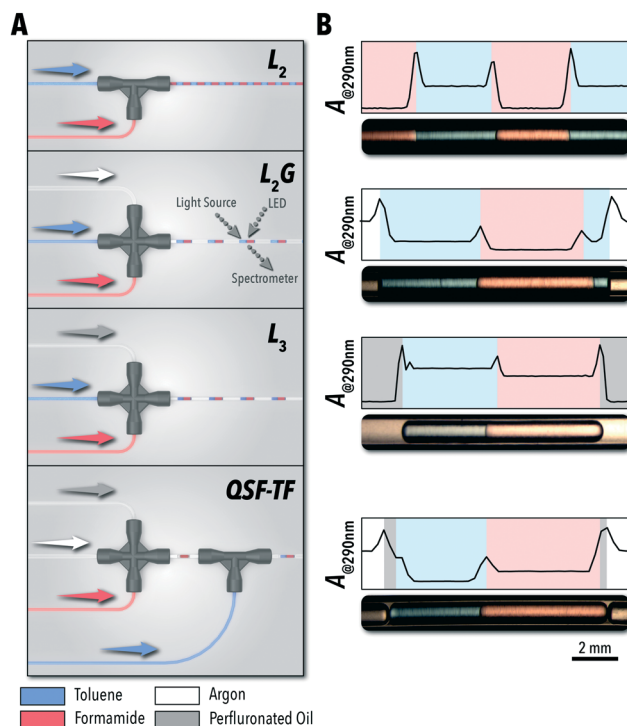

Fig. 1 Plug-and-play MF configurations. (A) Schematic of commercial fluidic junctions and fluoropolymer tubing configurations used to attain two- to four-phase segmented flow regimes. (B) Temporal absorption measurement at 290 nm for each of the sample flow regimes with corresponding representative images.

solvent (toluene), an inert carrier fluid (perfluorinated oil), and an inert gas phase (argon). All four flow configurations (Fig. 1A) were designed using commercially available fluidic junctions and fluoropolymer tubing (fluorinated ethylene propylene, FEP). The QSF system was operated in two microreactor configurations: the system shown in Fig. 1A, where toluene was injected into a L_2G formamide system (QSF-TF) and the reverse, where formamide was injected into toluene (QSF-FT). Compared to L_2G reactors with similar sequential injection formats, this QSF system does not require custom modifications to the fluoropolymer capillary tubing and uses only commercially available junctions.[16]

Flow stability of each system was evaluated through continuous *in situ* monitoring of the light absorption at 290 nm over time (Fig. 1B) – using a custom-developed flow cell[17,32] connected to a miniature spectrometer and broad-spectrum light source through fiber-optic patch cords – where each individual phase and interface could be identified through the changes in the absorption intensity. 290 nm was selected as the measurement wavelength due to the distinct absorption intensities produced by each of the phases used in this work with formamide as the reference.

In a continuous biphasic chemical process, the primary flow parameters relevant to the reaction are the reactive phase velocity (controlling the reaction time) and the volumetric ratio of the reactive solutions (R_1). Comprehensive and precise control of these two key parameters in flow can

significantly expand the experimentally accessible reaction parameter space. The remaining experimental parameter that may then be tuned to achieve stable MF is the ratio of the carrier phase to the total volumetric flow rate (R_2). The ratios R_1 and R_2 are defined according to the relations:

$$R_1 = \frac{Q_T}{Q_F + Q_T} \tag{1}$$

$$R_2 = \frac{Q_{Ar} + Q_O}{Q_{Ar} + Q_O + Q_F + Q_T} \tag{2}$$

where Q_T, Q_F, Q_{Ar}, and Q_O are the volumetric flow rates of toluene, formamide, argon, and perfluorinated oil, respectively. In two- and three-phase flow configurations, the irrelevant carrier phase is zero.

Five flow configurations were tested for segmentation stability across these three parameters, and the results are shown in Fig. 2A. In all three- and four-phase configurations, eight R_2 values uniformly spanning 0.3 to 0.8 were tested for each R_1 and velocity combination. The flow conditions were considered stable if the reactive phase solutions (toluene and formamide) combine in a uniform periodic pattern and the ratio of these two solutions within each droplet is uniform and representative of the input injection ratio. If any combination of parameters produced stable flow, the corresponding R_1-velocity pair is shown in the plot and the size of the point indicates the number of occurrences.

The L_2 and L_2G systems were highly stable across the full range of tested flow conditions; however, for many synthesis applications, these flow regimes are not viable options due to the common issue of microreactor fouling. In an exemplary biphasic reaction involving colloidal nanocrystals, that is the biphasic ligand exchange of sulfide anions with oleic acid-

capped CdSe QDs[33] – a reaction discussed in greater detail below – a continuous L_2G system resulted in significant microchannel fouling in a short period of time (Fig. 2B). Under ultra-violet (UV) illumination, fouling of the microreactor wall with QDs was observed after only one hour of operation with the L_2G format. Alternatively, the QSF system was able to continuously operate without any detectable QD accumulation in the microchannel. Under magnification of a sample biphasic reaction using the QSF format (Fig. 2C), the carrier oil phase can be seen forming a lubrication film between the reactive solution and the microchannel wall, enabling continuous operation of the biphasic reaction in flow regardless of the reactive phase propensity for fouling. It should be noted that the lubricating oil carrier phase can impact the performance of some biphasic reactive systems through partial absorption of reactive species at higher temperatures. Furthermore, the inclusions of the wetting film will alter the mass-transfer properties of the reactive phase. In a comparable L_2G system, where the reactive phase meets the reactor wall, there is likely to be a stronger recirculation pattern within the droplet.

Combining two variants of QSF applied in this study (QSF-FT – shown in Fig. 2D – and QSF-TF) can enable complete access to the tested operational space. As a general heuristic, the flow stability in the QSF systems is determined by the ratio of the injection between the two reactive solutions. The secondary injection volume, then, may not surpass approximately the volume of the initial reactive phase injection. In configuration QSF-TF, R_1 must be kept below 0.5. Conversely, for QSF-FT, R_1 must be kept above 0.5. By alternating between the two configurations, a stable flow may be established across the full tested range of velocities and R_1 values. While this simplified rule provides guidance to implement QSF into reaction studies, a more detailed
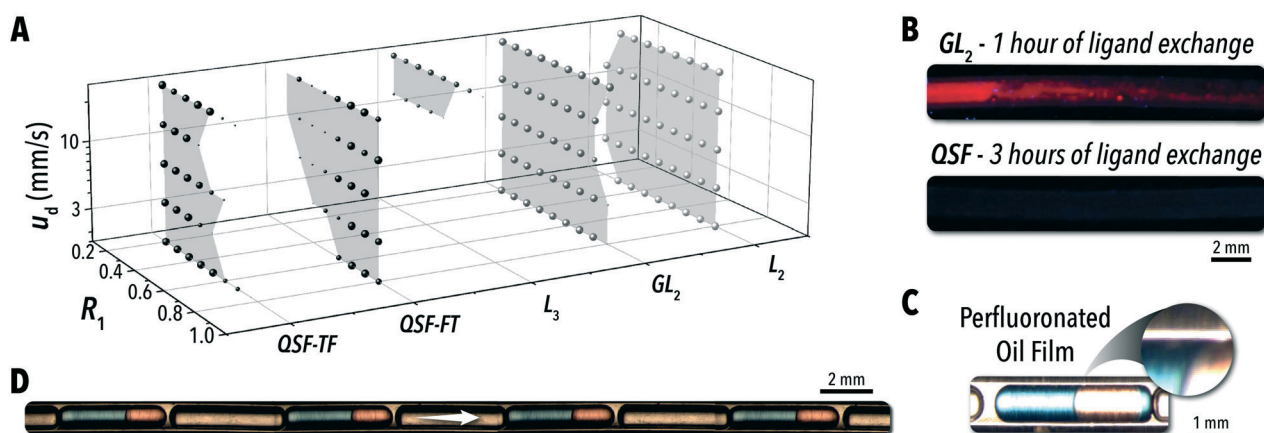

Fig. 2 Flow regime efficacy. (A) Illustration of stable flow regime regions across the reactive phase ratio (R_1) and reactive phase velocity, where stability is determined through absorption data at 290 nm across all available carrier to reactive phase ratios (R_2) and the scatter point size represents the proportion of R_2 values that resulted in stable flow. (B) Demonstration of fouling of the microchannel wall for a biphasic ligand exchange of CdSe QDs in a gas–liquid–liquid flow regime and corresponding four-phase microchannel through UV excitation after conducting experiments then clearing the capillary tubing with argon. (C) Bright-field image of oil film formed in four-phase flow regime, which allows for separation of the reactive phase from the microchannel wall, and (D) sample image of QSF system made through composite high resolution individual images.

understanding of the parameters dictating flow stability is required to access the full QSF operational space.

Typically, the two main factors controlling the flow uniformity in a microreactor are: (1) the injection rate of the carrier oil and (2) the secondary injection droplet formation frequency *versus* the gas phase segment passing time (t_p). Insufficient carrier oil injection rate not only risks fouling of the microchannel wall, similar to L_2G systems, but it can also result in flow instability. In a stable QSF operating regime, the inert gas phase inhibits immediate injection of the secondary injection droplet, causing passive synchronization of the injection into the primary droplet.[16,17,34] Without the presence of the inert gas phase, the injecting species will often prematurely form an isolated droplet, inhibiting contact between the reactive phases. Similarly, excessive carrier oil injection rates can result in two forms of flow instability. First, as shown in Fig. 3A, auxiliary oil slugs may form at the primary injection point due to the comparably low flow rate of the first

reactive species. This isolated oil slug will often provide a stable medium for encapsulating the secondary injection phase, causing an alternating formation of the biphasic reaction solution and isolated secondary reactant droplets. Due to the carrier oil's low surface energy, it will segment at a higher frequency than that of an equivalent flow rate of either reactive solution.[35] Therefore, it is important to balance the ratio of the primary injection reactive species with the carrier oil phase. Furthermore, if the carrier oil phase is able to fully encapsulate both reactive phases, high flowrates of a carrier oil phase fraction can cause separation of the reactive phases within the biphasic droplet.[16]

The dynamics of balancing the inert carrier fluid volumetric flow rate with the gas and reactive phase components are an important aspect in attaining stable MF. However, capturing the full complexity of the issue requires consideration of the fluid velocity, film formation dynamics, reactive species volume, and three-phase segmentation
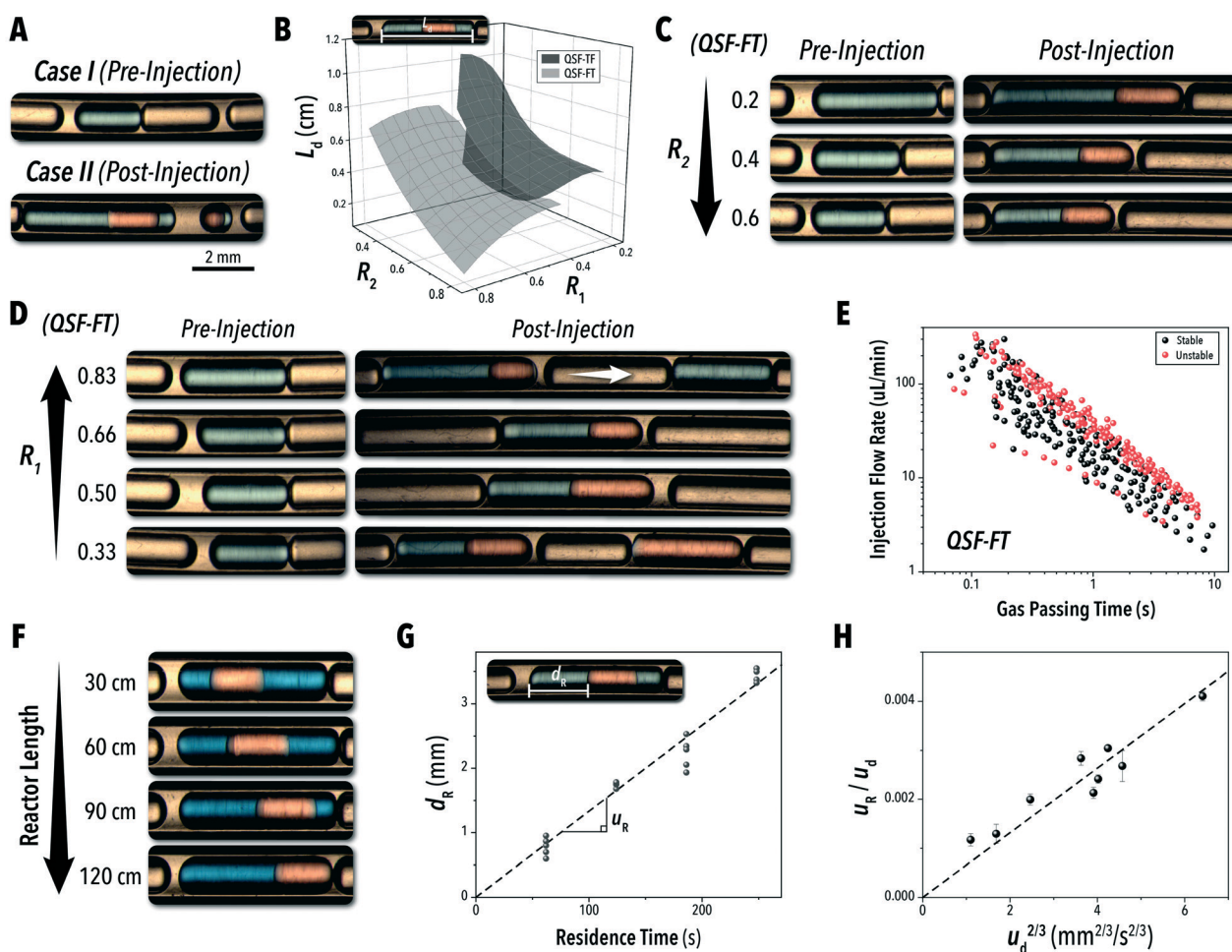

Fig. 3 Four-phase flow control. (A) Image of two instances in which excessive carrier oil flow rate will result in an unstable or functionally ineffective flow, (B) polynomial fit of slug length for both four-phase flow injection configurations, as determined by absorption data, (C) images demonstrating the effect of increasing the carrier to reactive phase ratio and (D) the ratio between the reactive phases on the initial and final flow segmentation, (E) four-phase flow secondary injection species flow rate as a function of absorption measured gas phase passing time for configuration QSF-FT where conditions measured as stable are black and unstable are red, (F) image of a single set of four-phase flow conditions at different points along the tube, and (G) the relative position of the encapsulated formamide phase as a function of time with (H) the corresponding relative velocity calculations as a function of the slug velocity to the two-thirds power.

principles. Full exploration of the topic extends beyond the scope of this study, but in our preliminary screening experiments, a carrier fluid to total reactive species volumetric flow ratio of 11–14% was found to be sufficient for the experimental conditions explored in this work.

While the total volumetric flow rate is the primary factor in calculating the droplet velocity – see ESI† section S.1 – the R_1 and R_2 values played a significant role in the reactive droplet volume (Fig. 3B), and R_1 largely dictated QSF stability. As shown in Fig. 3C, the droplet length (L_d) in the initial L_2G system may be tuned through adjusting the R_2 value[35] and the secondary injection adds the new reactive phase to the existing droplet at the preestablished segmentation frequency. The droplet segmentation frequency and length can further be controlled by switching between the QSF configurations. QSF-TF results in larger combined droplet length than those of QSF-FT at equivalent conditions. With capillary numbers (Ca = $\mu u_D/\sigma$, where u_D is the droplet velocity, μ is the dynamic viscosity, and σ is the surface tension) on the order of 10^{-4}, flow segmentation with the microchannel dimensions and fluid velocities explored in this study operates in the squeezing regime,[36] where parameters such as the surface tension and viscosity play a role in the droplet dimensions.[37] Among the fluid properties associated with Ca, formamide has a significantly higher dynamic viscosity than toluene.[38,39] Therefore, according to current droplet formation models[35] formamide would be expected to produce larger droplets at the initial cross-junction than toluene for the same volumetric injection rates. It should be noted that u_D is calculated assuming a plug flow velocity profile – i.e. the fluid velocity is constant across the full cross-section. However, due to the lubricating film formed by the carrier oil, the actual inner droplet velocity is expected to be slightly higher.

Outside of the influences of the inert carrier fluid, the main factors affecting QSF stability may be understood by comparing the injection rate of the secondary phase relative to the average gas phase passing time between droplets. Flow instability at this point occurs when the secondary injection rate is either higher or lower than the acceptable range for the given droplet formation frequency (Fig. 3D). To quantify this effect across the full parameter space, the gas passing time (t_P) was measured from the experimental absorption data used for the flow stability study presented in Fig. 2. As shown in Fig. 3E, there is a barrier in the maximum t_P as the flow rate of the injection species increases. Once t_P reaches a certain threshold, the secondary injection species begins to form unwanted auxiliary droplets, separate from the primary species. This additional injection reduces the measured gas passing time by splitting the gas phase into two separate sections. On the lower unstable region, the formamide injection is not high enough to break off from the T-junction at the rate necessary to fill each passing droplet uniformly. For the QSF-TF system, this lower bound was not observed at equivalent conditions (ESI† section S.2). Due to the larger droplet formation in the QSF-TF regime, the secondary

injection species is exposed to a longer gas passing time for every equivalent set of conditions. Furthermore, the toluene phase features a higher segmentation rate. For lower R_1 values, a similar boundary is expected to appear for the QSF-TF format. It should be noted that these studies and observations are designed around a single set of microchannel dimensions and pure solvents, and further analyses would likely allot greater control and range for other reactive systems.

An additional consideration for biphasic reaction applications is movement of the encapsulated reactive phase (i.e., formamide) within the biphasic droplet (i.e., toluene and formamide), as this movement will play an important role in the mass-transfer at the reactive interface. Mobility of the encapsulated reactive phase within the surrounding reactive species follows trends similar to that of an L_2G encapsulated system. By measuring the relative displacement of the formamide phase within the toluene over time (d_R, Fig. 3F and G), the relative velocity within the biphasic droplet could be calculated over several biphasic droplet velocities. The correlation of an L_2G system states that relative mobility is dependent on Ca according to the relationship below:[40]

$$\frac{u_R}{u_d} = m(\text{Ca})^{\frac{2}{3}} \tag{3}$$

where u_R is the relative velocity of the interior droplet and u_d is the velocity of the biphasic droplet. This correlation may then be simplified into:

$$\frac{u_R}{u_d} \propto (u_d)^{\frac{2}{3}} \tag{4}$$

As shown in Fig. 3H, the relative velocity follows a linear trend to the biphasic droplet velocity to the two-thirds power, indicating that a similar trend holds.

Biphasic reaction case study: continuous flow ligand exchange of CdSe QDs

To demonstrate the unique capabilities of the developed QSF format for continuous operation of biphasic reactions, we adapted the biphasic ligand exchange of oleic acid-capped CdSe QDs with sulfide ions.[24] In addition to introducing a continuous-flow ligand exchange reaction, within this case study, we also demonstrate the capability of continuous-flow photo-enhanced ligand exchange which produces S^{2-}-capped CdSe QDs with improved PL intensities.

The conventional technique for conducting biphasic ligand exchange reactions of colloidal QDs is through vigorous agitation of the reaction vessel via vortex mixer. Flask-based biphasic ligand exchange is not a scalable route as the extent of agitation necessary is highly energy and mechanically expensive. Stirring of the reaction vessel is then an unviable alternative. In-flow chemical synthesis allows for a facile scale-up through a numbered-up design of the
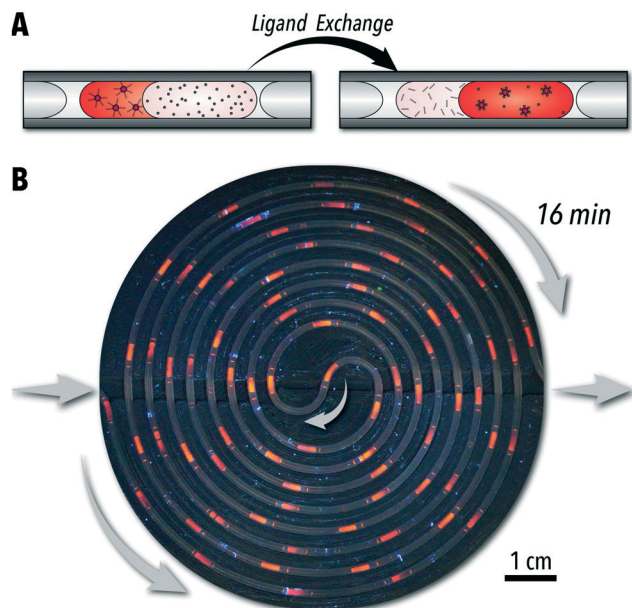
Fig. 4 Biphasic ligand exchange of CdSe QDs in flow. (A) Schematic of the biphasic ligand exchange process where oleic acid-capped CdSe QDs transitions from toluene to formamide to produce sulfide ligand-capped CdSe QDs. (B) Image of the continuous biphasic ligand exchange reaction in flow within the adjustable length spiral microreactor under UV illumination.

microreactors.[41] The QSF format can provide valuable insights into controlling reaction parameters affecting the

reaction kinetics, colloidal stability, and morphology of the nanocrystals during the biphasic ligand exchange reaction (*i.e.*, interfacial surface energy and diffusion rates). In addition, parameterizing biphasic and interfacial reactions in continuous flow formats is a necessary step towards automated, high-throughput reaction studies. Conducting the biphasic ligand exchange of CdSe QDs in a continuous QSF format, shown in Fig. 4A and B, offers both a scalable an intensified processing option for both laboratory- and large-scale continuous nanomanufacturing. Within this format, ligand exchange is accompanied by a phase transfer of CdSe QDs from toluene to a solution of sodium sulfide in formamide. *In situ* obtained absorption and PL spectra can be used to monitor CdSe QD properties, such as PL intensity, in each phase at different stages of the ligand exchange reaction. The extent of exchange can also be monitored by measuring the absorption value at 350 nm, which can be correlated to CdSe QD concentration. As shown in Fig. 5A and B, the in-flow biphasic ligand exchange process without UV excitation reaches completion in 16 min.

In addition to providing a scalable ligand exchange route, tubular flow reactors with a microchannel smaller than 1 mm also enable access to intensified photo-enabled processes through increased light penetration.[42] Moreover, each liquid slug will be exposed to the same amount of light as it passes along the reactor channel, regardless of flux uniformity across a surface. As shown in Fig. 4B, positioning the tubular flow reactor within a compact circular area allows for a high-power UV lamp (395 nm) to illuminate the entire flow reactor
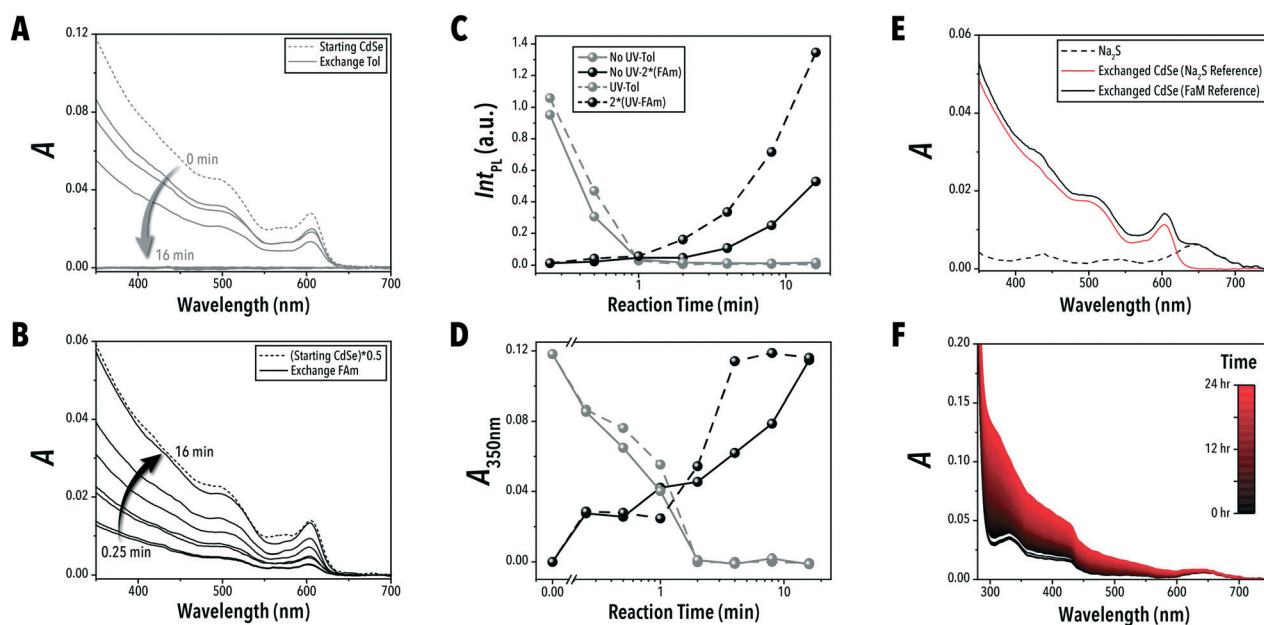

Fig. 5 Spectral monitoring of biphasic ligand exchange of CdSe QDs in flow. Time evolution of the UV-vis absorption spectra of the CdSe QDs in (A) toluene (Tol) and (B) formamide (FAm) phase with the absorption of the starting CdSe spectra and the starting CdSe spectra multiplied by 0.5 respectively for reference. (C) The relative integral photoluminescence intensity (Int_{PL}) and (D) absorption intensity of CdSe QDs at 350 nm (A_{350nm}) in the toluene and the formamide phase multiplied by two for volume correction ($2 \times$ (FAm)) with (UV) and without UV (no UV) exposure over time. UV-Vis absorption spectra of (E) sodium sulfide and ligand-exchanged CdSe QDs [16 min, no UV exposure] with sodium sulfide and with formamide as the references and (F) degassed sodium sulfide left stagnant in the microreactor, back-pressurized with argon over 24 h.

throughout the biphasic ligand exchange reaction and visualize the time-to-distance transformation along the flow direction. The microreactor design presented in this work enables adjustable tubing lengths within this constrained circular area – shown in ESI† section S.3. Interestingly, we observed that continuous UV illumination in this biphasic ligand exchange reaction can rapidly improve PL intensity of ligand-exchange nanocrystals, possibly due to photooxidation which can reduce surface trap states and structural defects at CdSe/CdS interfaces, as observed previously in batch reactors.[25,43,44] As shown in Fig. 5D and ESI† section S.4, for a similar ligand exchange concentration, the UV-passivated CdSe QDs achieved photoluminescence (PL) intensities 2.5 times higher than the QDs without UV illumination. Furthermore, the UV illumination decreased the time required for complete ligand exchange by four times (Fig. 5D). This, to our knowledge, is the first demonstration of photo-enhanced PL of CdSe QDs in a continuous flow format. Although the nature of this enhancement is outside the scope of this work, this platform may be used for further high-throughput investigations of ligand-mediated stokes-shift tuning, heterostructure formation, and PL enhancement of QDs.

The continuous QSF configuration provides an additional advantage unique to the biphasic ligand exchange reaction discussed in this study. The sodium sulfide nonahydrate in formamide precursor undergoes a slow degradation process at room temperature. The formed by-product compounds absorb light in the wavelength range that interferes with the wavelengths relevant to the CdSe QDs being studied – shown in Fig. 5E and F. Utilizing the aged sodium sulfide solution as an absorption reference instead of the pure solvent (formamide) allows for more accurate UV-vis absorption characterization of the biphasic ligand exchange process over time. The automated flow chemistry platform with the QSF reactor presented here enables the *in situ* monitoring of the sodium sulfide solution, allowing for continuously updated references to enable accurate spectral monitoring of the ligand-exchanged QDs.

Conclusions

The developed QSF format is a robust, reproducible, and readily employable multi-phase flow configuration for automated, high-throughput fundamental and applied studies of various biphasic chemical processes. The QSF flow strategy may be controlled for a wide range of reactive phase ratios and fluid velocities using simple flow selection heuristics, and it operates without the reactive phases in contact with the microchannel wall. Therefore, the QSF format offers robust and extended operation of biphasic chemical syntheses, which is critical for exploiting the advantages of automated experimental systems towards closed-loop autonomous experimentation systems. The continuous flow biphasic ligand exchange introduced in this work, demonstrated the efficacy of this MF format, while highlighting the advantages of continuous flow strategies partnered with photo-enhanced biphasic reactions. Further implementation of this technology could enable more efficient and controlled synthesis methods to produce high-quality solution-processable materials *via* biphasic and interfacial reactions, such as surface functionalized and anisotropic nanoparticles as well as alloy nanoclusters. Other biphasic reactions, such as those employing phase-transfer catalysts, may also benefit from comprehensive high-throughput reaction screening afforded by the QSF format. Most notably, the QSF format may extend biphasic reactions from fundamental studies to continuous processing with increased efficiency without the drawback of microreactor fouling found in L_2G and L_2 continuous flow systems.

Methods

Formamide (14835) was purchased from Alfa Aesar. Sudan red G (17373) was purchased from Sigma Millipore. Sodium sulfide nonahydrate (93-1183) was purchased from Strem Chemicals. Perfluorinated oil (Galden HT-200) was purchased from Kurt J. Lesker Company. Red dye (Allura Red AC) was purchased from McCormick. All chemicals were used as received.

All microcapillary tubing was comprised of fluorinated ethylene propylene (FEP) (IDEX H&S), where all feed lines had a 0.01″ inner diameter (ID) tubing and the microreactor channel and segment between the cross and tee junction were 0.03″ ID. The cross and tee junctions were polyether ether ketone (PEEK) (IDEX H&S). For absorption flow stability studies, 0.05″ ID cross and tee junctions were used as received, except for the QSF studies, which used a 0.06″ ID in the microchannels parallel to the flow direction. Additionally, the ligand exchange QSF studies implemented the modified tee along with a 0.0275″ ID cross junction for improved stability.

UV-vis absorption and photoluminescence spectra for stability and ligand exchange studies were collected with a miniature spectrometer (Ocean Insights, OCEAN-HDX-UV-VIS), broad spectrum light source (Ocean Insights, DH-2000-BAL), and high powered 365 nm LED (Thorlabs, M365LP1) connected to a custom inline sampling flow cell for 1/16″ outer diameter tubing[11] through fiber optic patch cords (Ocean Insights, P600-2-SR). Continuous UV illumination of the microreactor was conducted with a handheld lamp (Glossday, 100LED) positioned approximately 8″ from the flow reactor plate. The adjustable length, spiral tubing mount was 3D printed in polylactic acid (PLA), and the full model is included in the ESI (section S.3). OA-capped CdSe QDs were synthesized following a procedure adapted from Knauf *et al.* (see ESI† section S.5).[23] The sodium sulfide solution was prepared by first degassing 20 mL of formamide for one hour under vacuum, then 1.2 g of sodium sulfide nonahydrate was added to the mixture and degassed for one more hour before loading into a stainless-steel syringe (20 mL, Swagelok fitting) under inert atmosphere. Ligand exchange studies were conducted by flowing argon, carrier oil, starting CdSe in toluene, and sodium sulfide solution in formamide at flow rates of 27, 3, 5.3, and 10.6 µL min^{-1}, respectively, in the QSF-TF configuration.

Author contributions

Conceptualization A. A. V., M. A.; data curation A. A. V.; formal analysis A. A. V. (lead), R. W. E.; funding acquisition M. A.; investigation A. A. V.; methodology A. A. V.; project administration M. A.; resources D. Y., F. N. C., M. A.; software A. A. V., R. W. E. (lead); supervision M. A. (lead), F. N. C.; visualization A. A. V. (lead), R. W. E.; writing – original draft A. A. V.; writing – review & editing A. A. V., M. A. (lead).

Conflicts of interest

There are no conflicts to declare.

Acknowledgements

References

1 M. Maeki, in *Microfluidics for Pharmaceutical Applications: From Nano/Micro Systems Fabrication to Controlled Drug Delivery*, Elsevier, 2018, pp. 101–119.

2 C. Zhu, K. Raghuvanshi, C. W. Coley, D. Mason, J. Rodgers, M. E. Janka and M. Abolhasani, *Chem. Commun.*, 2018, **54**, 8567–8570.

3 K. Raghuvanshi, C. Zhu, M. Ramezani, S. Menegatti, E. E. Santiso, D. Mason, J. Rodgers, M. E. Janka and M. Abolhasani, *ACS Catal.*, 2020, **10**, 7535–7542.

4 Z. S. Campbell, M. Parker, A. Bennett, S. Yusuf, A. K. Al-Rashdi, J. Lustik, F. Li and M. Abolhasani, *Chem. Mater.*, 2018, **30**, 8948–8958.

5 R. W. Epps, M. S. Bowen, A. A. Volk, K. Abdel-Latif, S. Han, K. G. Reyes, A. Amassian and M. Abolhasani, *Adv. Mater.*, 2020, **32**, 2001626.

6 J. A. Bennett, Z. S. Campbell and M. Abolhasani, *React. Chem. Eng.*, 2019, **4**, 254–260.

7 S. Han, M. A. Kashfipour, M. Ramezani and M. Abolhasani, *Chem. Commun.*, 2020, **56**, 10593–10606.

8 A. A. Volk, R. W. Epps and M. Abolhasani, *Adv. Mater.*, 2021, **33**, 2004495.

9 Z. S. Campbell and M. Abolhasani, *React. Chem. Eng.*, 2020, **5**, 1198–1211.

10 Z. S. Campbell, F. Bateni, A. A. Volk, K. Abdel-Latif and M. Abolhasani, *Part. Part. Syst. Charact.*, 2020, **37**, 2000256.

11 Y. Li, R. K. Reddy, C. S. S. R. Kumar and K. Nandakumar, *Biomicrofluidics*, 2014, **8**, 054125.

12 Y. Fu, L. Bai, S. Zhao, X. Zhang, Y. Jin and Y. Cheng, *Chem. Eng. Sci.*, 2018, **181**, 79–89.

13 I. G. Lignos, R. C. R. Wootton, A. J. DeMello and B. M. Stone, in *Encyclopedia of Biophysics*, Springer Berlin Heidelberg, 2013, pp. 2300–2306.

14 I. Shestopalov, J. D. Tice and R. F. Ismagilov, *Lab Chip*, 2004, **4**, 316–321.

15 R. W. Epps, K. C. Felton, C. W. Coley and M. Abolhasani, *Lab Chip*, 2017, **17**, 4040–4047.

16 A. M. Nightingale, T. W. Phillips, J. H. Bannock and J. C. de Mello, *Nat. Commun.*, 2014, **5**, 3777.

17 K. Abdel-Latif, R. W. Epps, F. Bateni, S. Han, K. G. Reyes and M. Abolhasani, *Adv. Intell. Syst.*, 2021, **3**, 2000245.

18 R. W. Epps, A. A. Volk, K. G. Reyes and M. Abolhasani, *Chem. Sci.*, 2021, **12**, 6025–6036.

19 A. A. Volk and M. Abolhasani, *Trends Chem.*, 2021, **3**, 519–522.

20 C. Mateos, M. J. Nieves-Remacha and J. A. Rincón, *React. Chem. Eng.*, 2019, **4**, 1536–1544.

21 N. S. Eyke, B. A. Koscher and K. F. Jensen, *Trends Chem.*, 2021, **3**, 120–132.

22 F. Mekki-Berrada, Z. Ren, T. Huang, W. K. Wong, F. Zheng, J. Xie, I. P. S. Tian, S. Jayavelu, Z. Mahfoud, D. Bash, K. Hippalgaonkar, S. Khan, T. Buonassisi, Q. Li and X. Wang, *npj Comput. Mater.*, 2020, **7**, 1–10.

23 R. R. Knauf, J. C. Lennox and J. L. Dempsey, *Chem. Mater.*, 2016, **28**, 4762–4770.

24 A. Nag, M. V. Kovalenko, J. S. Lee, W. Liu, B. Spokoyny and D. V. Talapin, *J. Am. Chem. Soc.*, 2011, **133**, 10612–10620.

25 L. Liu, X. Zhang, L. Ji, H. Li, H. Yu, F. Xu, J. Hu, D. Yang and A. Dong, *RSC Adv.*, 2015, **5**, 90570–90577.

26 M. Saniepay, C. Mi, Z. Liu, E. P. Abel and R. Beaulac, *J. Am. Chem. Soc.*, 2018, **140**, 1725–1736.

27 K. Abdel-Latif, F. Bateni, S. Crouse and M. Abolhasani, *Matter*, 2020, **3**, 1053–1086.

28 Y. Ding, P. D. Howes and A. J. Demello, *Anal. Chem.*, 2020, **92**, 132–149.

29 J. Sui, J. Yan, D. Liu, K. Wang and G. Luo, *Small*, 2020, **16**, 1902828.

30 R. L. Hartman, *Org. Process Res. Dev.*, 2012, **16**, 870–887.

31 K.-J. Wu and S. Kuhn, *Chim. Oggi*, 2014, **32**, 62–66.

32 M. Abolhasani, C. W. Coley, L. Xie, O. Chen, M. G. Bawendi and K. F. Jensen, *Chem. Mater.*, 2015, **27**, 6131–6138.

33 Y. Shen, M. Abolhasani, Y. Chen, L. Xie, L. Yang, C. W. Coley, M. G. Bawendi and K. F. Jensen, *Angew. Chem., Int. Ed.*, 2017, **56**, 16333–16337.

34 D. Karan and S. A. Khan, *React. Chem. Eng.*, 2019, **4**, 1331–1340.

35 S. Haase, *Int. J. Multiphase Flow*, 2017, **88**, 251–269.

36 T. Fu and Y. Ma, *Chem. Eng. Sci.*, 2015, **135**, 343–372.

37 M. De menech, P. Garstecki, F. Jousse and H. A. Stone, *J. Fluid Mech.*, 2008, **595**, 141–161.

38 F. J. V. Santos, C. A. Nieto De Castro, J. H. Dymond, N. K. Dalaouti, M. J. Assael and A. Nagashima, *J. Phys. Chem. Ref. Data*, 2006, **35**, 1–8.

39 V. Campos, A. C. G. Marigliano and H. N. Sólimo, *J. Chem. Eng. Data*, 2008, **53**, 211–216.

40 M. Abolhasani, N. C. Bruno and K. F. Jensen, *Chem. Commun.*, 2015, **51**, 8916–8919.

41 J. Zhang, K. Wang, A. R. Teixeira, K. F. Jensen and G. Luo, *Annu. Rev. Chem. Biomol. Eng.*, 2017, **8**, 285–305.

42 C. Sambiagio and T. Noël, *Trends Chem.*, 2020, **2**, 92–106.

43 K. J. Schnitzenbaumer and G. Dukovic, *J. Phys. Chem. C*, 2014, **118**, 28170–28178.

44 M. V. Llopis, J. C. C. Rodríguez, F. J. F. Martín, A. M. Coto, M. T. Fernández-Argüelles, J. M. Costa-Fernández and A. Sanz-Medel, *Nanotechnology*, 2011, **22**, 385703.